Chemical Papers (2022) 76:7357–7372
https://doi.org/10.1007/s11696-022-02411-w

ORIGINAL PAPER

Biosorption of methyl orange from aqueous solution with hemp waste, investigation of isotherm, kinetic and thermodynamic studies and modeling using multigene genetic programming

Nurşah Kütük[1] · Sibel Arslan[2]

Received: 7 April 2022 / Accepted: 3 August 2022 / Published online: 16 August 2022

Abstract
Water resources around the world are getting polluted day by day due to the rapidly developing industry. Industrial wastes have caused serious damage to the environment in recent years. Especially, dyes are waste products that mix with waters such as lakes, rivers and seas and have toxic and carcinogenic effects. In this study, the removal of methyl orange (MO) dye, which was chosen as a model dye compound, from aqueous solution by biosorption using hemp waste was investigated. The biosorption process was optimized by the parameters of pH, initial dye concentration and amount of biosorbent. Biosorption of MO to hemp waste was investigated by isotherms, kinetics and thermodynamic studies. It was determined that the biosorption equilibrium fitted to the Langmuir isotherm (R^2=0.9739). As a result of the experimental studies, 83% biosorption value and 1428 mg/g maximum biosorption capacity were reached with 250 mg/L dye concentration and 0.5 g/L biosorbent amount at pH = 2. It was determined that the reaction kinetics were in accordance with the pseudo-second-order kinetics (R^2 =0.9911). In addition to, the study aims to evaluate to what extent the modeling of the biosorption process is successful. For this purpose, we used multigene genetic programming (MGGP), which has been renewed with the latest developments in the field of model extraction. The results show that MGGP is efficient for modeling the biosorption process in real environments. The analysis of MGGP models also showed that pH is the most important parameter affecting the biosorption process.

Keywords Biosorption · Hemp wastes · Methyl orange · Genetic programming · Multi-gene genetic programming

Introduction

Water pollution is a serious problem affecting the ecosystem and people all over the world. One of the most important reasons is dye waste (Khwannimit et al. 2020). Dyes have been used for many years in various fields such as food, textile, automotive, medical and cosmetic industries (Arici 2021). Even a small amount of the dyes can be seen in water and harms the ecosystem by preventing light transmission (Joudi et al. 2020). Azo dyes are anionic and contain nitrogen–nitrogen double bonds ($-N=N-$) in their structure. They have a complex aromatic structure, and the biodegradability of azo dyes is poor (Subbaiah and Kim 2016). Due to the aromatic ring structure, the dyes are carcinogenic and harmful (Su et al. 2014). For example, MO is a water-soluble, synthetic anionic and monoazo dye used in various fields such as paper, food and medicine. It is a toxic, carcinogenic and teratogenic dye with harmful effects such as jaundice, vomiting and cyanosis in humans. It also harms aquatic life and soil by disturbing the ecological balance. Therefore, the removal of MO, which is a frequently used dye in the industrial field, from residual water is important for human and environmental health (Lafi et al. 2020; Arici 2021; Wu et al. 2021). Various techniques such as coagulation, flocculation, flotation, oxidation, ozonation, ion exchange, precipitation, membrane separation, photocatalysis, and adsorption are used for the removal of dyes from wastewater (Lafi et al. 2020; Subbaiah and Kim 2016). Most of these methods are effective and efficient, but costly and difficult to implement. Adsorption

✉ Nurşah Kütük
nkutuk@cumhuriyet.edu.tr

Sibel Arslan
sibelarslan@cumhuriyet.edu.tr

[1] Faculty of Engineering, Department of Chemical Engineering, Sivas Cumhuriyet University, Sivas, Turkey

[2] Faculty of Technology, Department of Software Engineering, Sivas Cumhuriyet University, Sivas, Turkey

is a cheap, simple technique that is easy to apply. In addition, the use of a variety of adsorbents has led researchers to the adsorption technique (Wu et al. 2021). Biosorption uses many materials that are inexpensive, environmentally friendly and readily available (Azeez and Al-zuhairi 2021). These biosorbents include various materials such as palm ash, rice husks, neem sawdust and pumpkin seeds (Subbaiah and Kim 2016). Hemp fiber is known as Cannabis sativa. It is an important plant used in various fields such as medicine, textile and pharmaceuticals (Berni et al. 2021; Dinçel 2022). Hemp contains bioactive constituents such as flavonoids, saponins and alkaloids (Zhu et al. 2021). Studies show that hemp has good sorption properties and reported that hemp fiber is a successful sorbent for the removal of Zn(II) ion from aqueous solution. In addition, hemp has been reported to have good biomass and biodiesel properties (Tofan et al. 2016). In a study using papaya fiber, MO was removed from aqueous solution at pH 2 and after 120 min (Ahmaruzzaman 2012). In Bayazit's work, magnetic multi-wall carbon nanotubes (MWCNT) was used to removal MO from aqueous solution. The adsorption value of 98% was reached when the magnetic was modified with Fe_3O_4 (Bayazit 2014). It is possible to examine the parameters affecting the removal of dyes or heavy metals from wastewater with various data programs. Assasi et al. modeled the photocatalytic degradation of crystal violet dye with a ZnO photocatalyst with the Box–Behnken experimental design and investigated the factors affecting the degradation rate (Assassi et al. 2021). In another study, an empirical model was created for the nickel removal of fig biosorbent from wastewater with a full factorial design. pH and biosorbent mass were determined to be important among the parameters affecting the biosorption process (Madjene et al. 2016). Similarly, in the response surface method using the Box–Behnken model, the adsorption pH, initial dye concentration and adsorbent dose variables of the ciprofoxacin antibiotic were optimized (Nguyen and Van 2022). Activated sludge was used as a biosorbent in a study when the removal of pharmaceutical wastes in waste materials was examined (Runjavec, et al. 2022).

Genetic programming (GP) is a field of evolutionary computation that automatically searches for parameters and nonlinear equations to find the optimal formula to represent a system. Nowadays, many complicated problems in engineering (Ashofteh et al. 2015; Keshavarz and Mehramiri 2015) (Li and Wong 2015), commerce (Fallahpour et al. 2016), production planning (Nguyen et al. 2017) and other problems in computer science such as computer vision (Liu et al. 2016), signal processing (Feli and Abdali-Mohammadi 2019) and artificial neural network design (Suganuma et al. 2018) can be solved using GP. The widespread use of GP in many disciplines and fields is mainly due to its flexible and understandable structures. Moreover, many studies have shown that GP is more successful than various methods such as ANN and SVM (Muduli et al. 2015; Muduli and Das 2014; Pan et al. 2013). Therefore, in this study, the prediction performance and frequency of inputs of the experimental data were evaluated using multigene GP, the most widely used version of GP.

Biosorption of MO dye from an aqueous solution was investigated using hemp waste as a biosorbent that we know has not been used before. Hemp waste was directly used as a biosorbent without chemical treatment due to its fibrous structure, environmental friendliness, and to evaluate natural wastes. For this purpose, the effects of pH, initial dye concentration, biosorbent dose and temperature parameters on the biosorption process were studied. Equilibrium with Langmuir, Freundlich and Harkins–Jura isotherms, first-order reaction kinetics, second-order reaction kinetics, intraparticle diffusion and Elovich model kinetics and reaction kinetics were investigated. In addition, we successfully applied GP, which supports the study of parameter effects in modeling the biosorption process. So, in summary, impressive performance along with real experimental data is an important goal in modeling biosorption processes using the GP method. The main contributions of this study are twofold:

- To the best of our knowledge, we are the first to propose multigene genetic programming-based modeling for the biosorption of MO in hemp waste as part of an evolutionary learning process.
- Hemp waste was evaluated by using it to remove environmentally harmful MO.

As a result, it is thought that this study will fill a gap in the literature and make a significant contribution with the use of hemp waste for MO removal from aqueous solution for the first time and MGGP modeling.

Experimental

Materials

The methyl orange used in the study was obtained from Surechem Product, and hydrochloric acid (HCl, 33%) and sodium hydroxide (NaOH, pellet) were obtained from Kimetsan. Waste hemp grown for fiber production in the Amasya-Turkey region was obtained from ATC-Hawk. Figure 1a, b shows the hemp plant and its harvest in the field. Table 1 includes the physicochemical properties, structure and maximum absorbance wavelength of the dye.

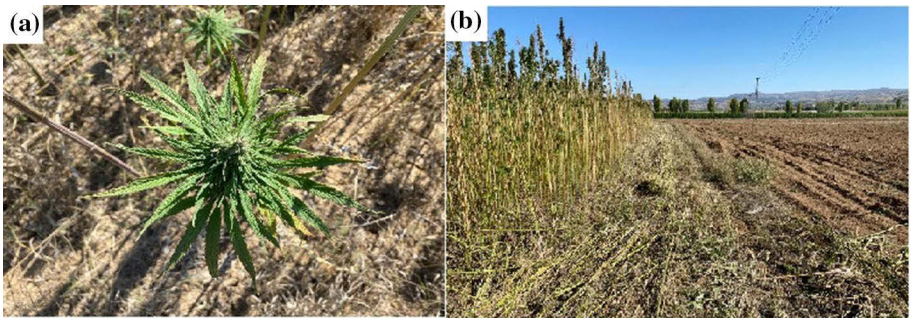

Fig. 1 **a** Hemp plant and **b** hemp harvested in the field

Table 1 Properties of dye

Dye	Methyl orange
Chemicals formula	$C_{14}H_{14}N_3NaO_3S$
Molecule weight (g/mol)	327.34
Ionic structure	Anionic
Solubility	High (for water)
Color	Red-Yellow
λmax	464 nm
IUPAC nomenclature	4-dimethylamino-noazobenzene-4'-sulfonic acid

Biosorption procedure

The size of the hemp waste separated into its fibers was reduced by 0.5–2 mm using a grinding machine (EMIR industrial kitchen products, model EMR-Q-01) to increase the contact area. The aqueous methyl orange solution was first prepared as a stock solution with a concentration of 1000 mg/L. Then it was diluted and prepared at the specified concentrations. The experiments were performed intermittently in a 250-mL glass flask and 100 mL dye volume. Samples taken at specified time intervals were filtered. Then, the absorbance values were determined at 464 nm by UV–Vis spectroscopy. In the biosorption studies, dye removal was optimized by the parameters of pH (2–8), dye concentration (10–250 mg/L), biosorbent amount (0.5–10 g/L), contact time (0–240 min) and temperature (25–50 °C).

$$\%\text{Biosorption} = \frac{\text{Co} - \text{C}}{\text{Co}} \times 100 \tag{1}$$

In the equation, *Co* is the initial concentration of the dye (mg/L) and *C* is the concentration (mg/L) at time t.

The biosorption capacity of hemp wastes is calculated according to the following Eqs. 2 and 3.

$$q_e = \frac{(\text{Co} - \text{Ce}).\text{V}}{\text{m}} \tag{2}$$

$$q_t = \frac{((\text{Co} - Ct).V)}{m} \tag{3}$$

In Eqs. 2 and 3, q_e is the biosorption capacity (mg/g) at equilibrium, q_t is the biosorption capacity (mg/g) at $t = t$, Ce is the final concentration (mg/L), V is the solution volume (mL), and m is the biosorbent amount (g). Biosorption experiments were repeated three times.

Characterization

To investigate the relationship between hemp waste and the dye MO, chemical structure analysis was performed using a the attenuated total reflection Fourier transform infrared spectroscopy (ATR-FTIR) spectrophotometer (Bruker, Tensor II) in the range 4000–400 cm^{-1}. Morphological images were obtained using Tescan Mira 3 XMU scanning electron microscopy (SEM) instrument. Absorbance values of the dye MO were determined by ultraviolet (UV) spectroscopy (Schimadzu 1601).

Genetic programming

GP is the pioneer of automatic programming methods and is the basis of the genetic algorithm (GA). It was introduced in 1985 by Cramer (1985) and further developed by Koza (1994). The steps of the algorithm of GP are similar to those of GA. The most fundamental difference between the methods is the representation of the solutions. While GA represents the solutions as fixed code sequences, GP represents them as parse trees whose structure consists of a combination of terminals and functions. The smallest unit of trees is called a node in GP. The nodes are selected from the set of terminals (variables and constants such as *x* and *y*) and the set of functions (arithmetic operators, logical functions, mathematical functions) defined specifically for the problems.

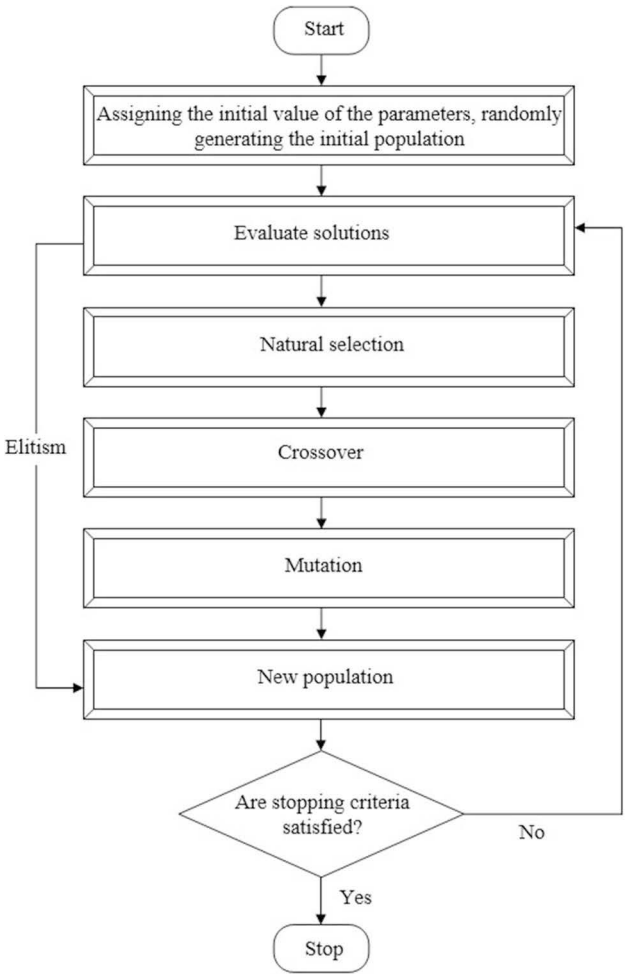

Fig. 2 Genetic programming flowchart

The flowchart GP is shown in Fig. 2. The first step of the flowchart is to create the initial population. The work of the natural selection operator, crossover operator and mutation operator in GA is adapted to GP to improve existing solutions and search for new solutions (Poli et al. 2008). The natural selection operator evaluates the fitness of each individual in the population for the problem. In all cases, the fitness of the individual is determined by running a specific fitness function and analyzing the entire tree (Gan et al. 2009). Individuals that have a good fitness value are more likely to be represented in the next generation. In the crossover operator, individuals with two parents are selected from the population based on their fitness. The mutation operator is randomly determined from the selected individual mutation point/node with fitness-based probability and allows searching for new, unseen and unexplored solutions (Karaboğa 2017). The best solutions of the generation are transferred to the current generation in elitism. The program is terminated when the given termination criteria (such as the specific fitness value of the solutions and the number of iterations) are met.

In addition to the standard GP, several versions of this type of automatic programming have been described in the literature, including multigene GP (MGGP) (Searson et al. 2010), geometric semantic GP (Moraglio et al. 2012) and gene expression programming (Ferreira 2001). In this study, MGGP is also briefly mentioned because it is studied using MGGP, one of the most commonly used versions.

Table 2 Solution of MGGP model

Genes	Genotype	Weight	Phenotype
	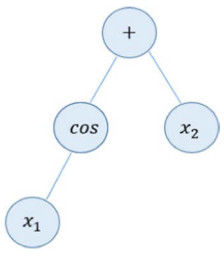	0.47	$\cos(x_1) + x_2$
	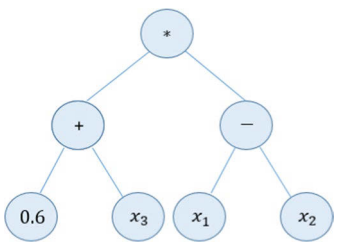	−0.23	$(0.6 + x_3) * (x_1 - x_2)$
Overall model	$y = 0.47 * (\cos(x_1) + x_2) - 0.23 * (0.6 + x_3) * (x_1 - x_2)$		

multi-gene genetic programming (MGGP)

MGGP is a widely used version of GP, which, unlike the standard models of GP, allows the use of multiple trees. In MGGP, each model is a linear combination of one or more trees. Each tree can be considered as part of a sub-model that makes a significant contribution to the overall model. In the model, the tree is called the "genotype" and the decoded and simplified tree structure is called the "phenotype" (Searson et al. 2010). Table 2 shows a solution for an MGGP model. The mathematical model of the trees representing the solution corresponds to sub-equations, where x_1,x_2 and x_3 are defined as independent variables and $f(x_1, x_2, x_3)$ is defined as the dependent variable. These sub-equations form the general equation by using the coefficient for each bias and other w coefficients.

Results and discussion

ATR-FTIR analysis

Functional groups from biosorption can be determined by ATR-FTIR analysis. The FTIR spectra of hemp waste and MO adsorbed hemp waste are shown in Fig. 3. The peak at 3338 cm^{-1} of hemp waste indicates the O–H stretch, and the peak at 2916 cm^{-1} represents the C–H stretch and is due to the cellulose structure (Dai and Fan 2010). It increases the wettability of the O–H function of hemp waste. This may provide an advantage as a biosorbent (Viscusi et al. 2019). It is attributed to the acetyl and uronic ester groups from the peak hemicellulose structure that appeared in 1737 cm^{-1} (Abraham et al. 2016). The peaks at 1423, 1371, 1320, and 1238 cm^{-1} represent the H–C–H plane vibration, plane C–H stretching, CH_2 stretching and C=O stretching of the cellulose structure, respectively. In turn, the peaks at 1032 and 560 cm^{-1} are due to the cellulose structure and

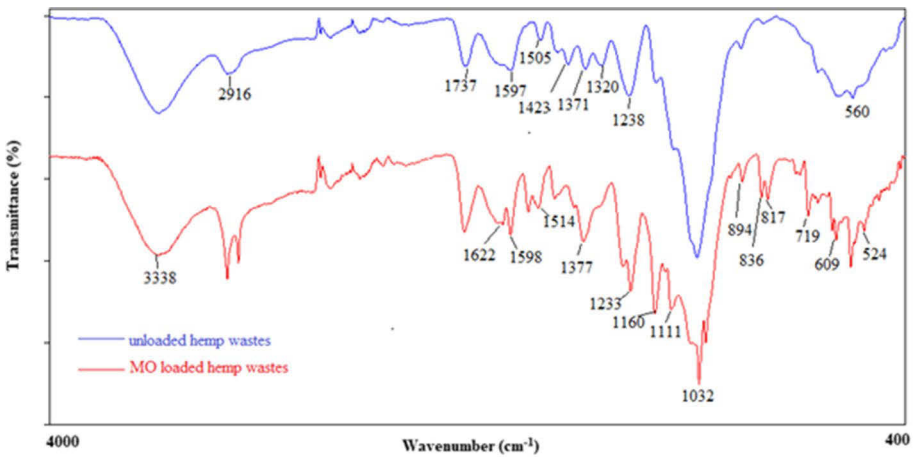

Fig. 3 FTIR spectrum of hemp wastes before and after biosorption of MO

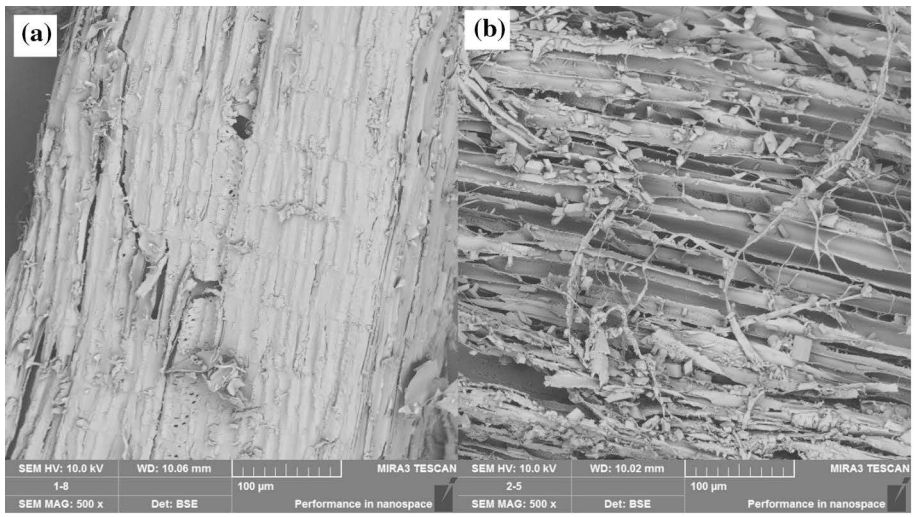

Fig. 4 SEM images of **a** unloaded hemp wastes and **b** MO-loaded hemp wastes

represent C–C stretching and C–OH out-of-plane bending bonds, respectively (Dai and Fan 2010). When the FTIR spectrum of the MO-loaded hemp waste was examined after MO biosorption, some new peaks were observed. The peaks at 1111 cm^{-1} and 1160 cm^{-1} are attributed to the –S=O and $–CH_3$ bonds of the MO structure. The peak occurring at 1622 cm^{-1} is related to the N=N group. Small peaks between 524 cm^{-1} and 894 cm^{-1} that occur after biosorption are in the fingerprint region (Bayazit 2014).

SEM analysis

The morphology of the surface structure was studied to test the usefulness of hemp waste as a biosorbent. SEM images of hemp waste before and after biosorption with MO are shown in Fig. 4. The smooth fibrous structure of hemp waste before biosorption attracts attention (Chimeni et al. 2018). It can be clearly seen that the hemp waste swells in its fibrous and regular structure after biosorption of the dye MO.

Parameters affecting biosorption

The pH of the dye solution is important because it changes the surface properties of the adsorbent, the degree of ionization and the color of the dye. Figure 5a shows the effects of pH on biosorption capacity (q_e) and biosorption (%). MO has a negative charge when the solution pH is less than 3.4. In addition, when MO dissolves in water, it forms continuous anions due to the sulfonate group in its structure. The resulting anions want to react with positive charges. Therefore, the biosorption value of MO dye increases in acidic conditions (Lafi et al. 2020). The best removal of MO from an aqueous solution was achieved with 53% biosorption (q_e =2.54 mg/g) at pH = 2. The biosorption values reached at pH 4, 6 and 8, respectively, were determined as 44%, 38% and 34%. As a result, it can be assumed that hemp waste adsorbs MO better in acidic medium. Biosorption value and biosorption capacity decrease with increasing pH.

The initial dye concentration is an important parameter for the biosorption process. It has been reported that adsorption capacity increases with dye concentration (Ahmaruzzaman 2012). In the study, different concentrations of dye solution (10, 25, 50, 100 and 250 mg/L) were used to investigate the effects of initial dye concentration. The pH of the dye solution was maintained at 2, and 0.1 g/L amount of hemp waste biosorbent was used. The results show that the initial dye concentration increases proportionally with biosorption capacity (Fig. 5b). The maximum biosorption capacity (122.51 mg/g) was reached when the dye concentration was 250 mg/L. Similarly, a biosorption value of 76% was

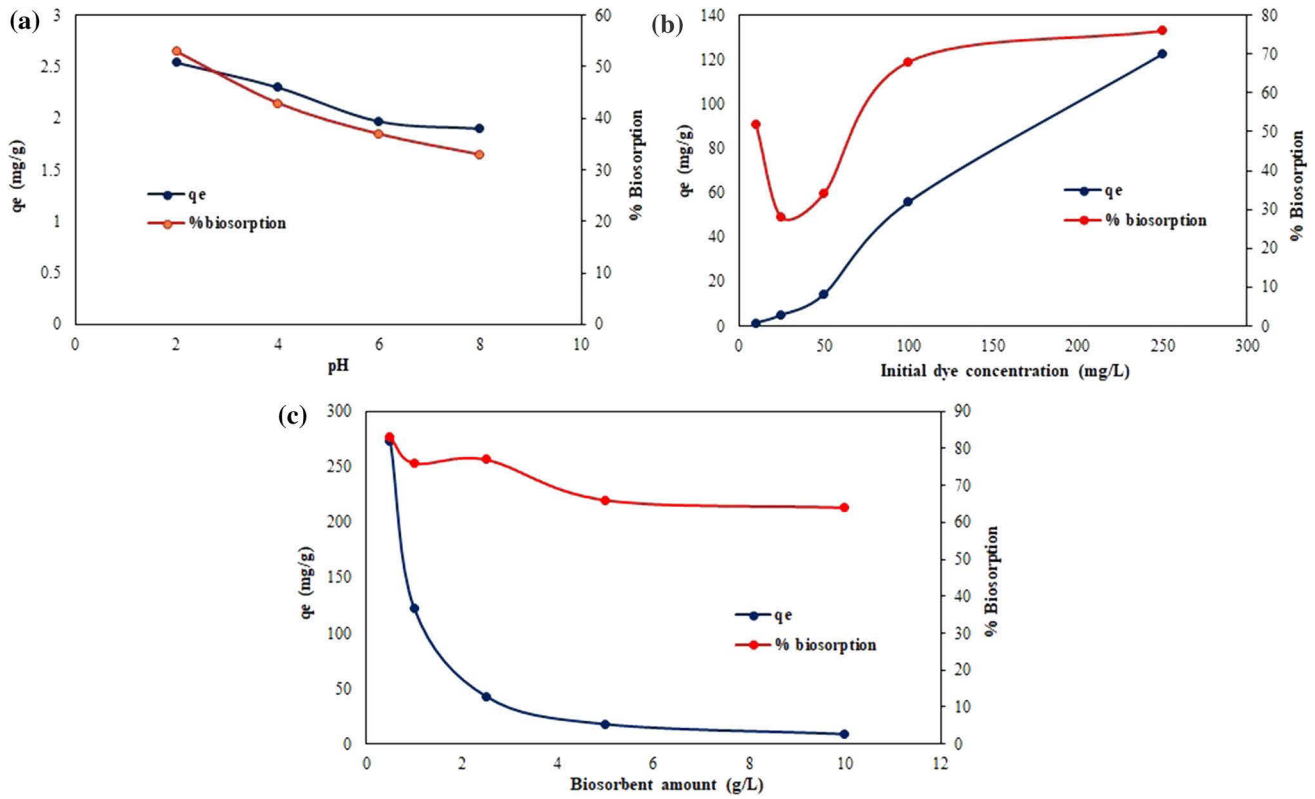

Fig. 5 % Biosorption vs biosorption capacity (q_e) **a** pH, **b** initial dye concentration, **c** biosorbent amount

achieved. In agreement with the literature, it can be said that high concentration of MO increases biosorption (Darwish et al. 2019).

Hemp waste was used in amounts of 0.5, 1, 2.5, 5 and 10 g/L to determine the appropriate biosorbent amount for the biosorption process. The initial dye concentration was adjusted to 250 mg/L and a pH of 2. It can be seen in Fig. 5c that the biosorption capacity decreases as the amount of biosorbent increases. The amount of biosorption decreases slightly. Although the biosorption did not change significantly with increasing amount of biosorbent, a decrease in biosorption capacity was observed. A biosorption capacity of 274 mg/g and a biosorption of 83% were achieved at the amount of 0.5 g/L hemp waste. At an amount of 10 g/L of biosorbent, a capacity of 9 mg/g was reached. The reason for this is that as the amount of biosorbent increases, the active sites responsible for adsorption on the surface increase proportionally. Because the active sites increase in number, they overlap, the diffusion distance increases and it may be difficult for the dye molecules to reach the active sites. For this reason, it is thought that the biosorption capacity decreases as the amount of biosorbent increases (Su et al. 2014; Mahmoodi et al. 2016; Lafi et al. 2020).

Biosorption isotherm models

Biosorption isotherms obtained at different concentrations provide information about the capacity of the biosorbent, surface properties and adsorption mechanism. In this study, Langmuir, Freundlich and Harkins–Jura isotherms were used to investigate the equilibrium mechanism in the biosorption of MO by hemp waste. The Langmuir isotherm states that adsorption is monolayer and homogeneous on the surface of the adsorbent. The Freundlich isotherm states that the adsorbent surface is heterogeneous and there is multilayer adsorption (Li et al. 2015). The Harkins–Jura isotherm indicates multilayer biosorption and heterogeneous pore distribution on the biosorbent surface (Liu and Wang 2013; Okpara et al. 2021). The Langmuir isotherm is shown in the following Eq. 4. K_L (L/mg) is the Langmuir constant, and $q$max (mg/g) is the maximum biosorption capacity. In Eq. 5, R_L shows the dimensionless equilibrium parameter. The R_L constant is used to determine the fitness of the Langmuir isotherm. The isotherm is not favorable if R_L is greater than 1, linear if equal to 1, favorable if 0 to 1 and irreversible if equal to 0. The Freundlich isotherm is shown in Eq. 6. Here K_f is the Freundlich constant. Similarly, $1/n$ is a Freundlich constant related to biosorption. Biosorption is efficient if $1/n$ is between 0 and 1 (Darwish et al. 2019; Okpara et al. 2021).

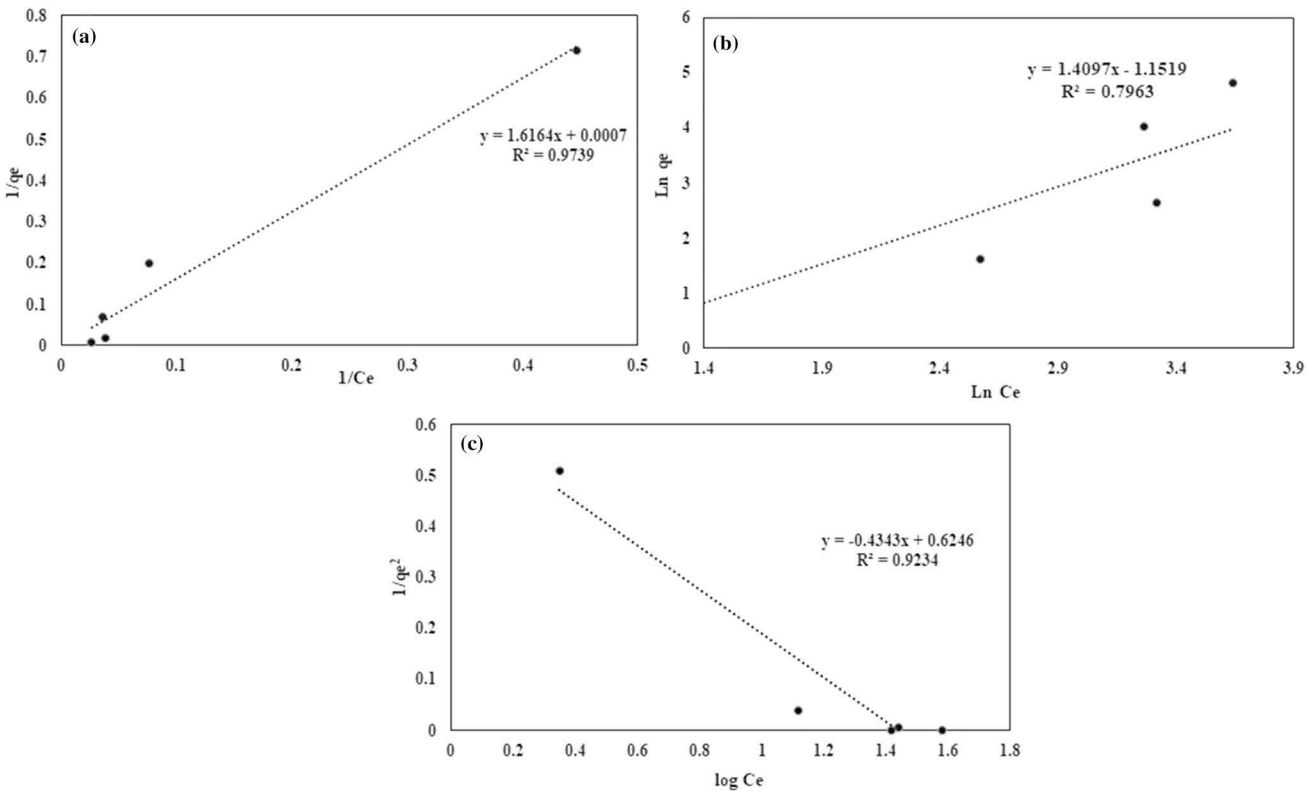

Fig. 6 **a** Langmuir isotherm model, **b** Freundlich isotherm, **c** Harkins–Jura model

Table 3 Data of Langmuir, Freundlich and Harkins-Jura isotherms

Isotherm	Value
Langmuir	
R^2	0.9739
R_L	0.9
q_{max} (mg/g)	1428
K_L (L/mg)	0.0004
Freundlich	
R^2	0.7963
$1/n$	1.4097
kF(L/g)	0.31
Harkins-Jura	
R^2	0.9234
A_H (g^2/L)	2.3
B_H (mg^2/L)	1.436

The Harkins–Jura isotherm is given in Eq. 7. A_H and B_H are Harkins–Jura isotherm constants (Liu and Wang 2013).

$$\frac{1}{\mathrm{qe}} = \frac{1}{q\mathrm{max}} + \left(\frac{1}{K_L.q\mathrm{max}}\right)\left(\frac{1}{\mathrm{Ce}}\right) \tag{4}$$

$$R_L = \frac{1}{1 + \mathrm{KL.Co}} \tag{5}$$

$$\mathrm{Lnqe} = \mathrm{LnKf} + \left(\frac{1}{n}\right)\mathrm{LnCe} \tag{6}$$

$$\frac{1}{\mathrm{qe}^2} = \frac{B_H}{A_H} - \left(\frac{1}{A_H}\right) logC_e \tag{7}$$

In Fig. 6a, b, c, graphs of Langmuir, Freundlich and Harkins–Jura isotherms, respectively, and in Table 3, the data calculated using the graph are given. Based on the high R^2 value (0.9739) of the Langmuir isotherm, it can be concluded that it is a monolayer adsorption mechanism. In addition, the distribution of active sites of hemp waste is homogeneous (Table 3). The highest biosorption capacity (q_{max}) value obtained from the Langmuir isotherm was calculated as 1428 mg/g. According to these results, the biosorption process is compatible with the Langmuir isotherm. A R_L value of 0.9 indicates that the biosorption system is favorable (Magdy et al. 2018). Since the Freundlich isotherm R^2 value is 0.8051, it can be said that the isotherm of the biosorption process fits. However, it is less compatible than the Langmuir isotherm. In this case, the biosorbent surface is heterogeneous and has good biosorption property. The high regression value (R^2 = 0.9234) of the Harkins–Jura isotherm indicates multilayer biosorption on the hemp surface and the presence of heterogeneous pores on the surface (Okpara et al. 2021).

In the biosorption of MO on hemp waste, the initial dye concentration has a significant effect on the biosorption capacity. In the Table 4, the biosorption capacity of hemp waste is compared with literature data. It can be seen that the biosorption capacity of hemp waste is quite high. This could be due to its fibrous structure. The fact that hemp waste is naturally occurring and has a high biosorption capacity without any modification makes it an important biosorbent.

Kinetic models

The effect of contact time with the biosorbent was studied in the range of 0–240 min (pH = 2, 250 mg/L initial dye concentration, 0.5 g/L of biosorbent). Biosorption kinetics were studied using pseudo-first-order reaction kinetics (Eq. 8), pseudo-second-order reaction (Eq. 9), intra-particle diffusion (Eq. 10) and Elovich model (Eq. 11) kinetics. Respectively, k_1, k_2, k_{id}, α and β are the reaction rate constants according to the models and are calculated and given in Table 5.

$$\log\left(q_e - q_t\right) = logq_e - \frac{k_1}{2.303}\,t \tag{8}$$

Table 4 Comparison of hemp waste with other sorbents for maximum sorption capacity (q_{max}) of MO

Sorbent	q_{max}, (mg/g)	References
Modified extracted cellulose	16.94	Lafi et al. (2020)
Wheat straw	50.4	Su et al. (2014)
NiO-NPs	97.56	Riaz et al. (2022)
Bentonite modified Ni–Fe layered double hydroxide	215.9	Sriram et al. (2022)
Fe_3O_4 MNPs	277. 14	Azeez and Al-zuhairi (2021)
Papaya leaf	333.34	Ahmaruzzaman (2012)
Hemp wastes	1428	This study

Table 5 Data of kinetic models

Kinetic models	Parameters	Value
Pseudo-first order	R^2	0.3787
	q_t(mg/g)	23.24
	q_e (mg/g)	23.89
	$k_{1(}$$min^{-1}$$_{)}$	0.015
Pseudo-second order	R^2	0.9911
	q_t(mg/g)	136.8
	q_e (mg/g)	140.84
	k_2 (g/mg.min)	0.002
Intra-particle diffusion	R^2	0.5927
	k_i(mg/g.min^2)	16.661
Elovich	R^2	0.8299
	β(g/mg)	0.018

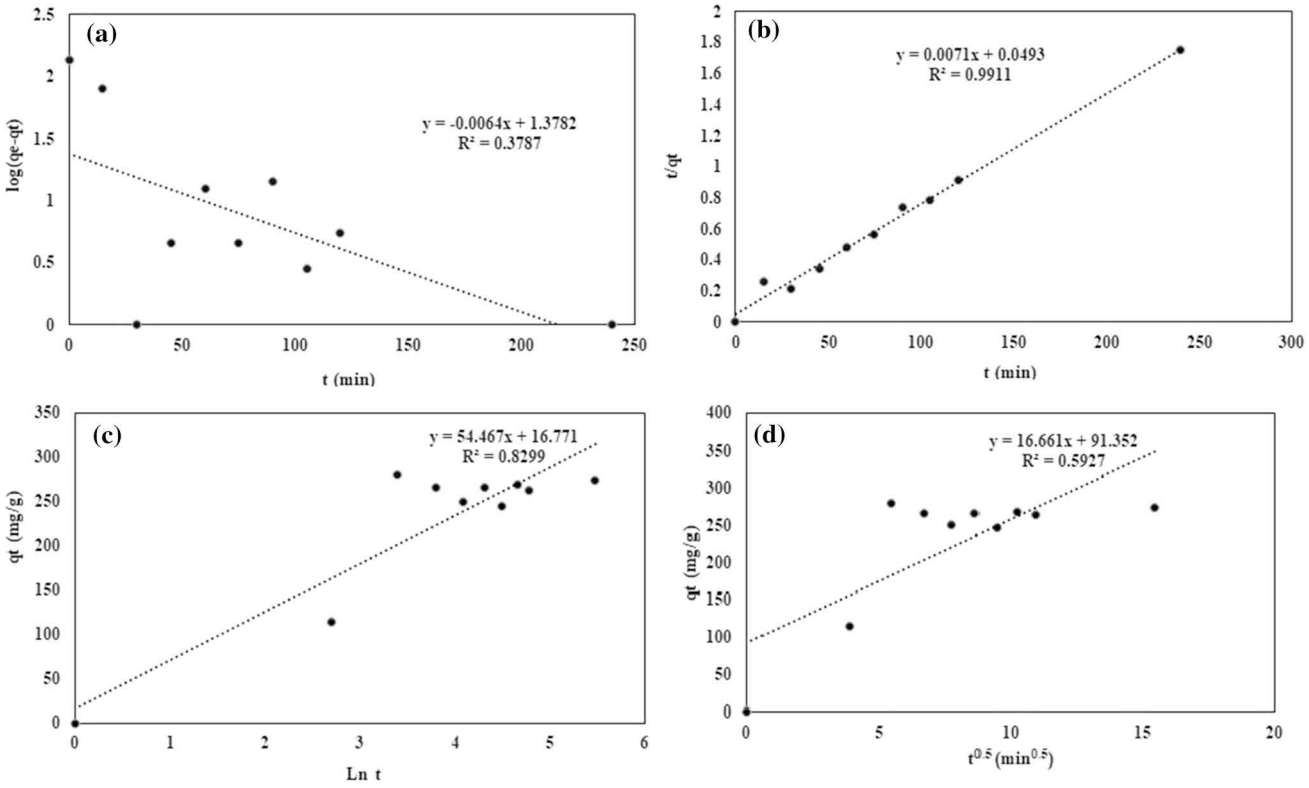

Fig. 7 Biosorption kinetics of hemp wastes **a** pseudo-first order, **b** pseudo-second order, **c** Elovich, **d** intra-particle diffusion

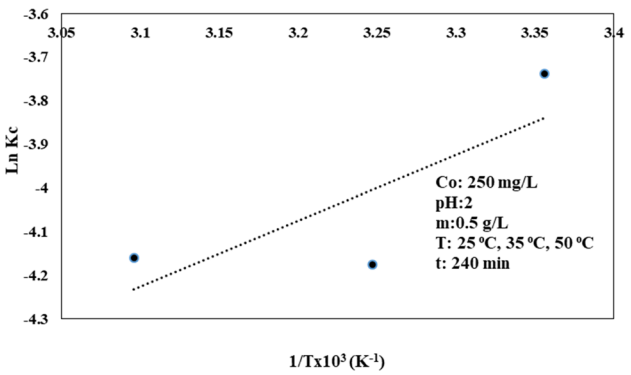

Fig. 8 Biosorption thermodynamic

$$\frac{t}{q_t} = \frac{1}{k_2.q_e 2} + \frac{1}{q_e}t \tag{9}$$

$$q_t = k_{id} \cdot t^{1/2} + \mathrm{C} \tag{10}$$

$$q_t = \frac{1}{\beta}\ln(\alpha.\beta) + \frac{1}{\beta}\ln t \tag{11}$$

The reaction kinetics for the biosorption process were investigated at pH 2, for an initial dye concentration of 250 mg/L, 0.5 g/L of hemp waste and a contact time of 240 min. By evaluating the experimental data with kinetic models, it was found that the biosorption kinetics agreed well with the pseudo-second-order kinetic model for hemp waste (Fig. 7b). Biosorption was found to follow the pseudo-second-order kinetic model. Representation of the biosorption kinetics of MO to hemp with second-order reaction kinetics indicates the presence of chemisorption (Sriram et al. 2022). On the other hand, the Elovich kinetic model expresses ion exchange; since the R^2 value is 0.8299, ion exchange can also be mentioned (Su et al. 2014). Regression values of first-order reaction kinetics ($R^2 = 0.3787$) and intra-particle diffusion model ($R^2 = 0.5927$) are low. While these results confirm the existence of a chemical type of biosorption between hemp waste and MO, it is thought that ion exchange may also occur.

Biosorption thermodynamic

To examine the effect of temperature on the biosorption of MO to hemp, the biosorption process at 25, 35 and 50 °C temperatures was investigated (Fig. 8). Thermodynamic parameters enthalpy energy (ΔH, kJ/mol), entropy change (ΔS, kJ/mol.K) and free energy change (ΔG, kJ/mol) data were calculated according to Eqs. 12, 13, 14. The graph in

Fig. 8 is obtained according to the Van't Hoff equation in Eq. 13.

$$K_c = C_a/C_e \tag{12}$$

$$InK_c = \frac{\Delta S}{R} - \frac{\Delta H}{R}.\frac{1}{T} \tag{13}$$

$$\Delta G = \Delta H - T\Delta S \tag{14}$$

Here, K_c is the equilibrium constant, C_a is the amount of dye retained in unit mass of biosorbent (mg/g), and C_e is the dye concentration remaining in solution (mg/L). Ideal gas constant R is taken as 8.314 J/mol K.

ΔH value was calculated as − 0.18 kJ/mol, and ΔS value was calculated as − 1.072 kJ/mol.K. The ΔG value calculated for 25, 35 and 50 °C temperatures was determined as 319.2, 330 and 346.07 kJ/mol, respectively. ΔH and ΔS values are negative in the results obtained. These results show that biosorption exhibits exothermic behavior and has a decreasing entropy characteristic. Positive ΔG values indicate that biosorption will not occur spontaneously and its applicability is low with increasing temperature (Azeez and Al-zuhairi 2021; Joudi et al. 2020).

The biosorption values obtained at 25, 35 and 50 °C were 83%, 72% and 71%, respectively. In accordance with the thermodynamic data results, increasing temperature decreased the biosorption. Conditions affecting biosorption were also investigated with GP in addition to experimental results. Due to the negative effect of the temperature increase on the biosorption process, the temperature value was taken as 25 °C in GP input values. The GP model was operated on the experimental data obtained at 25 °C.

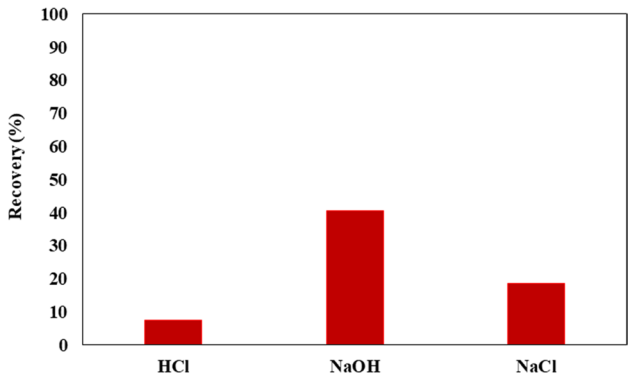

Fig. 9 Desorption of MO with different solvents (pH 2, Co : 250 mg/L, m: 0.05 g, contact time: 240 min, temperature 25 °C)

Desorption capacity

At the end of the optimized biosorption process in the last part of the experimental study, the desorption capacity of the MO-loaded hemp waste biosorbent was investigated. First, the dye-loaded biosorbent was filtered and dried in an oven at 40 °C for 24 h. It was then used in desorption experiments. The hemp waste biosorbent was regenerated in HCl, NaOH and NaCl aqueous solutions (0.1 mol/L each) for 240 min. At the end of the desorption experiments, the solution was filtered by filtration and the biosorbent was separated from the solution. The amount of desorption was determined by reading the absorbance of the sample taken from the remaining solution in UV spectroscopy at 464 nm. The amount of desorption was determined according to Eq. 15.

$$Desorption = (q_{\mathrm{des}}/q_{\mathrm{ads}}) \times 100 \tag{15}$$

Here q_{des} is the amount of MO desorbed (mg/g).

In this way, the results for both the recovery of MO and the reusability of the biosorbent are given in Fig. 9. According to the results, the desorption of the biosorbent was obtained in minimum HCl solution (7.5%) and maximum NaOH solution (40.6%). According to these results, hemp waste is a low cost and usable sorbent for removal and recovery of MO dye from aqueous solutions.

Modeling the biosorption process with MGGP

In this section, we present the experimental results of MGGP using a dataset. First, we explain the dataset used and then go into detail about the experimental setup of the current study. Finally, we present the results obtained with the dataset.

Dataset

As mentioned earlier, the goal of this study is to build a model that describes the relationship between input and output features. The dataset is partitioned based on the data partitioning widely used in machine learning (70% training and 30% test samples). The total number of samples in the dataset is 123, so 86 randomly selected samples (about 70%) were used for training and the remaining 37 samples (about 30%) were used for testing. Each data sample has 6 features: (x_1) pH, (x_2) initial dye concentration (mg/L), (x_3) biosorbent amount (g), (x_4) contact time (min), (x_5) temperature (°C), (y) biosorption (%). The biosorption is the target feature (y) and should be predicted from other features.

Table 6 Parameters

Parameters	GP
Population size	500
Initialization	Ramped half and half
Maximum tree depth	4
Crossover rate	0.84
Mutation rate	0.14
Direct reproduction rate	0.02
Maximum number of gen	6
Functions	times, minus, plus, rdivide (protected), square, tan, exp,log, mult3, add3, cube, negexp, neg, abs

Table 7 Simulation results of GP

Metrics	Best fitness	R^2_{train}	R^2_{test}
Mean	7.84	0.90	0.94
Best	5.92	0.95	0.96
Worst	8.84	0.88	0.88
Standard Deviation	0.56	0.01	0.02

Fitness function and parameters

We used the algorithm MGGP to improve the predictive performance of the removal proses modeling. The performance of the models is evaluated using the root-mean-square error (RMSE) on both the training set and the test set. The fitness function is shown in Eq. (16).

$$\text{RMSE} = \sqrt{\frac{1}{N}\sum_{i=1}^{N}\left(f\left(x_i\right) - Y_i\right)^2} \tag{16}$$

where N is the number of samples, $f\left(x_i\right)$ is the outputs of the extracted models and Y_i is the real outputs. The complexity of the solution trees obtained by the methods is calculated by Eq. (17) in proportion to the number of nodes and the depth of the trees.

$$C = \sum_{k=1}^{d} n * k \tag{17}$$

where C is the complexity of the tree, d is the depth of the tree and n is the total number of nodes in the corresponding depth of the tree. In addition, the performance of the modeling was statistically evaluated by the coefficient of determination (goodness of fit, R^2) using Eq. (18):

$$R^2 = 1 - \frac{\sum_{i=1}^{N}\left(f\left(x_i\right) - Y_i\right)^2}{\sum_{i=1}^{N}\left(Y_i - \overline{\text{Y}}\right)^2} \tag{18}$$

where N is the number of samples, $f\left(x_i\right)$ and Y_i are the predicted and real y values of sample i, respectively, and $\overline{\text{Y}}$ is the mean of the real output values. Other parameter values used in GP are listed in Table 6. The divide(/) function in the function set is a reserved version where the value of the divisor equals 0 and is later corrected to 1. Otherwise, a normal division is performed. The function square defines the square of a number, the function *cube* is the third power of a number, the function mult3 is the multiplication of three variables (x_1* x_2*x_3), and the function add3 is the sum of three (x_1+ x_2+x_3) used in the runs. Also, $neg(-x)$ and negexp(exp($-x$)) are defined. It was decided to use the parameters listed in Table 6 by trying different parameters.

Modeling results with MGGP

The simulation results in Table 7 are obtained by independently testing MGGP with 100 runs of 500 iterations each. In the experiments, the data were not normalized because the samples in the data set are more successful with non-normalized data. However, the dataset is randomly shuffled to monitor the success of the algorithm with unseen data. When evaluating the simulation results, it can be seen that many of the models have a R^2_{train} value close to 1, indicating a good fit to the training data. This means that the models provide a very good approximation to the problem function in the region of interest.

Figures 10 and 11 show how well the best model fits the training and test data, respectively.

Equation (19) shows the best overall model of all runs performed by GP. The best model in all runs builds x_1, x_2, x_3, x_4 parameters. The temperature parameter is not included in the model. Information about the complexity of the model can be found in Table 8, and the relationship between gene weights is shown in Fig. 12. As shown in Fig. 12, the best model consists of 6 genes and the second gene has absolute size compared to the other genes. In addition, using the p-value, we highlight the bias coefficient of the model and all genes are less than 0.05 at a 95% confidence level, which makes it significant and necessary for the model.

$$\begin{aligned} y = {} & 5563\text{e}^{-\frac{\sqrt{x_2}}{\tanh(x_4)}} - 21.28ln\left(\ln\left(x_1\right)\right) \\ & + 90.75tanh\left(x_3^2x_4^2\right) - 32.79tanh\left(\frac{0.8722x_2}{x_4}\right) \\ & - 6.625e + 5tanh\left(\frac{0.0046\tanh\left(x_4\right)}{x_2}\right) \\ & + 0.06485x_1^3 - 0.06485x_1x_3x_4 + 24.23 \end{aligned} \tag{19}$$

The expression complexity in Table 8 is calculated using Eq. (17). The total number of nodes in all genes was 38, which is an ideal number for a model of complexity. It is

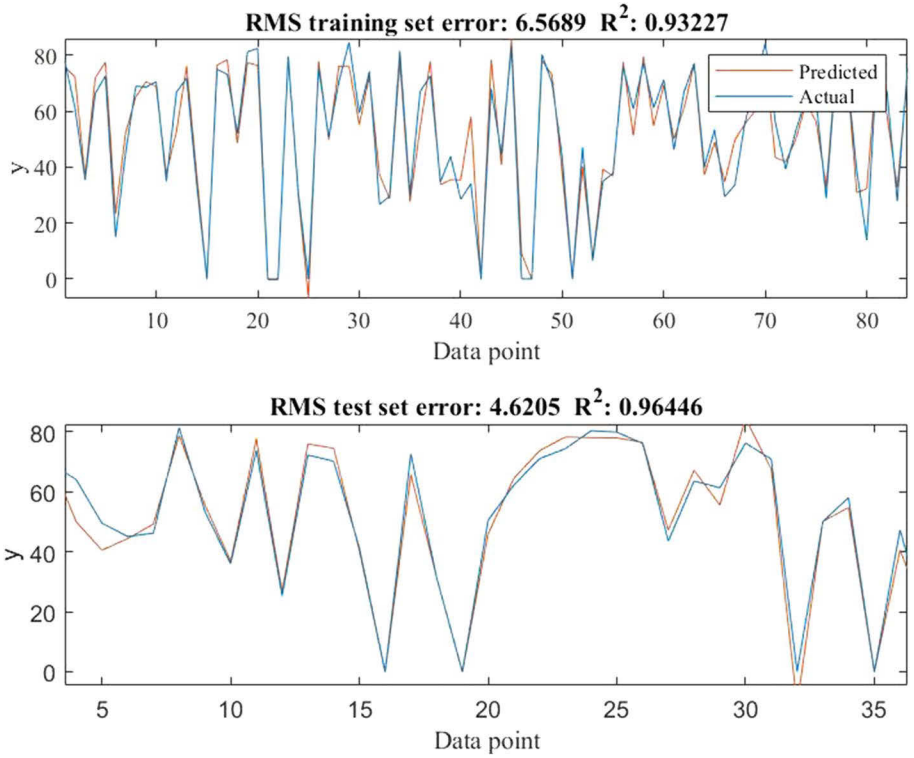

Fig. 10 Multi-gene regression the best model prediction

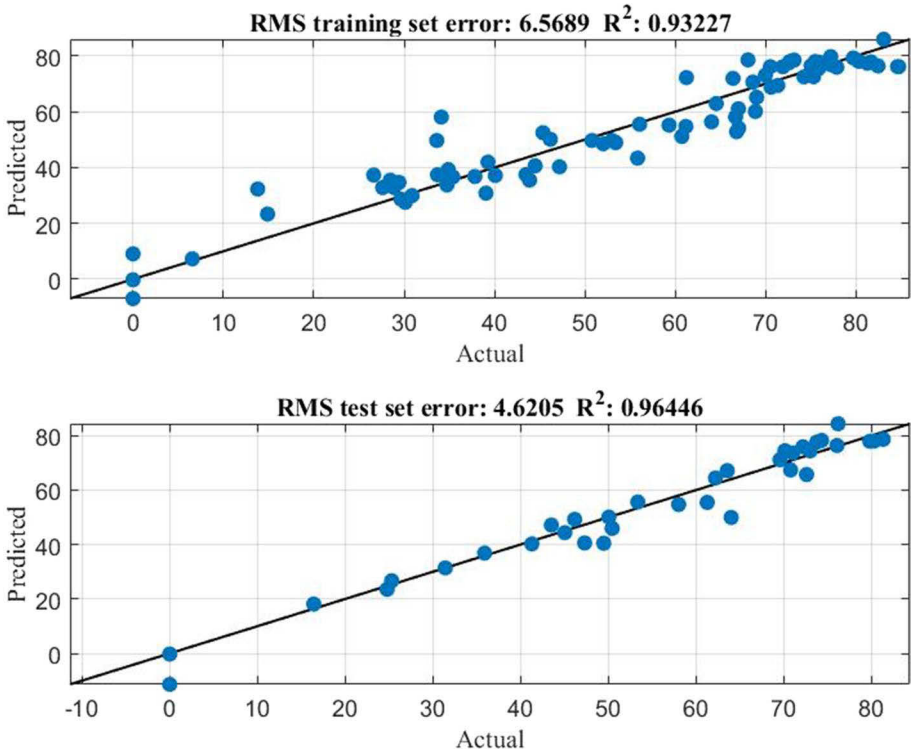

Fig. 11 Multi-gene regression the best model prediction scatterplot

Table 8 Structural properties relating to MGGP model representation

Description	Value
Genes	6
Nodes	38
Expressional complexity	111
Depth	4
Inputs	4
Inputs used	x_1,x_2,x_3,x_4

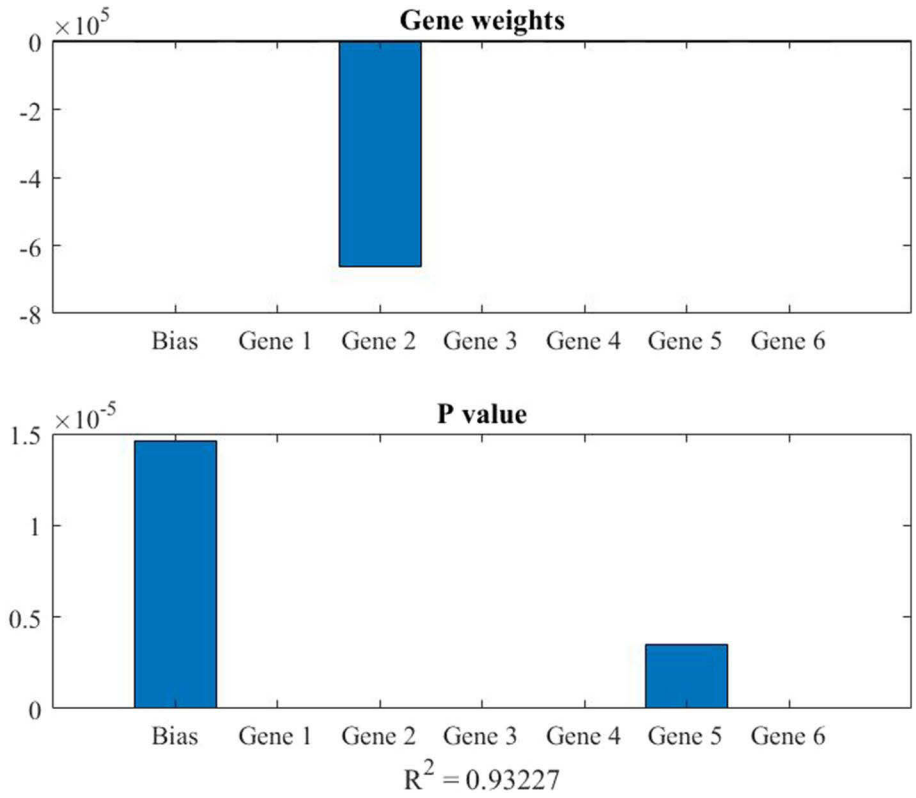

Fig. 12 Gene weights of the best model

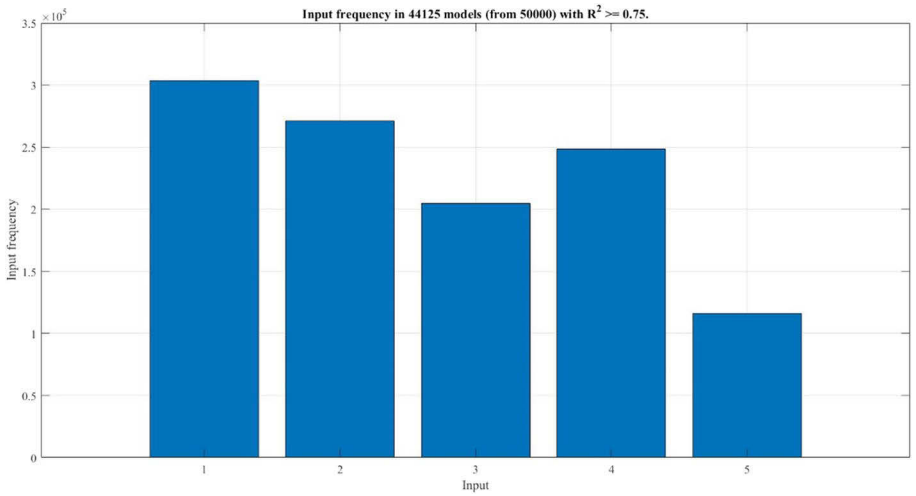

Fig. 13 Population input frequency of all runs ($R^2_{\text{train}} \geq 0.75$)

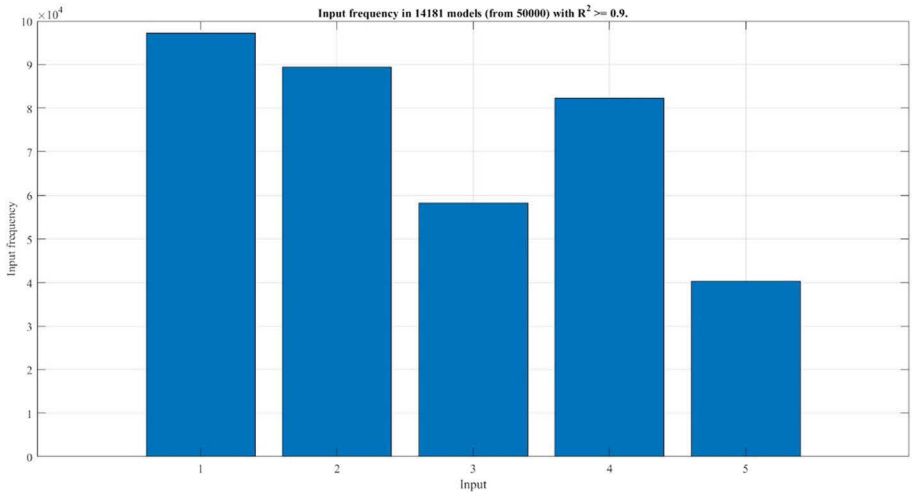

Fig. 14 Population input frequency of all runs ($R^2_{\text{train}} \geq 0.90$)

clear that all parameters except temperature are included in the mathematical equation of the best model. Also we visualize at the frequency distribution of input variables in all best models from 100 runs, which are represented by R^2_{train} in Figs. 13 and 14. An R^2_{train} value of 0.75 in our experiment indicates that 75% of the variance of the studied dependent output variable ((*y*) biosorption) is explained by the variance of the independent input variables ((x_1) pH, (x_2) initial dye concentration, (x_3) biosorbent amount, (x_4) contact time, (x_5) temperature). Therefore, in Figs. 13 and 14, frequencies were calculated over the most successful models of the experiments with R^2_{train} values of 0.75 and 0.9, respectively.

The population size of each run is 500. The population size of a total of 100 runs is 500*100 = 50,000. In other words, Figs. 13 and 14 are obtained by evaluating 50,000 different individuals. Among these 50,000 individuals, there are 44,125 individuals with R^2_{train} value greater than 0.75 and 14,181 individuals with R^2_{train} value greater than 0.9. When the input frequencies of 44,125 individuals are evaluated, the frequency of occurrence of parameters in models is x_1, x_2, x_4, x_3,x_5 from strong to weak. Also, the input frequencies of 14,181 individuals have the same order. When both graphs are evaluated together, it is concluded that the most important input for this dataset is x_1 (pH).

Conclusion

In this study, the biosorption mechanism of MO, an anionic dye from hemp waste, was investigated, and hemp waste was selected as the biosorbent. It was found that hemp waste achieved 83% biosorption at a pH of 2, an initial dye concentration of 250 mg/L, 0.5 g/L biosorbent, and a contact time of 240 min. The results of FTIR and SEM show that MO is biosorbed in fibrous hemp waste. The biosorption process was consistent with pseudo-second-order reaction kinetics. Biosorption in homogeneous monolayers and on heterogeneous surfaces was performed according to the isotherms of Langmuir, Freundlich and Harkins–Jura. A very high $q_{\max}$ value of 1428 mg/g was obtained in the biosorption process of the MO dye of hemp waste. Desorption studies of hemp waste showed 40.6% dye recovery in NaOH solution, and hemp waste is a recyclable biosorbent. It was concluded that the use of hemp waste will provide an advantage both in recycling vegetable wastes and in the fight against water pollution. In addition to, hemp waste can be placed inside structures of certain sizes (e.g., pipes, ropes and metal or glass rods) rather than dumped directly into irrigated areas. Thus, when the structural element is removed from the water, the dye-loaded biosorbent is separated in the water.

We also extracted the modeling of the biosorption process. In doing so, we have compared the results of the model obtained using the MGGP with the results obtained from real experiments. Our proposed MGGP models validated on real experiments have achieved superior performance and have shown high R^2 values in the obtained results. The model results are in agreement with the experimental data. In this case, apart from the temperature (because it is a constant value), the amount of biosorbent was the parameter that had the least effect on the biosorption in the experimental data. Although the amount of biosorbent affected the biosorption capacity in the experimental results, it did not significantly affect the biosorption. The most influential parameters are pH, initial dye concentration and contact time. In future, we plan to use the hemp waste biosorbent for the removal of other dyes and heavy metals.

The original aspect of this study is the use of the wastes of the hemp plant, which has just started production in Turkey, to remove MO dye from the aqueous solution, while the other is the successful model obtained by multigene genetic programming of the parameters affecting the process.

Funding The authors did not receive support from any organization for the submitted work.

Declarations

Conflict of interest There are no conflicts to declare.

References

Abraham RE, Wong CS, Puri M (2016) Enrichment of cellulosic waste hemp (*Cannabis sativa*) hurd into non-toxic microfibres. Materials. https://doi.org/10.3390/MA9070562

Ahmaruzzaman M (2012) Removal of methyl orange from aqueous solution using activated papaya leaf. Sep Sci Technol 47(16):2381–2390. https://doi.org/10.1080/01496395.2012.671432

Arici TA (2021) CTAB/H_2O_2 modified biosorbent for anionic dye from aqueous solutions: biosorption parameters and mechanism. Biomass Convers Biorefin. https://doi.org/10.1007/s13399-021-01920-0

Ashofteh PS, Haddad OB, Loáiciga HA (2015) Evaluation of climatic-change impacts on multiobjective reservoir operation with multiobjective genetic programming. J Water Resour Plan 141(11):04015030. https://doi.org/10.1061/(asce)wr.1943-5452.0000540

Assassi M, Madjene F, Harchouche S, Boulfiza H (2021) Photocatalytic treatment of crystal violet in aqueous solution: Box-Behnken optimization and degradation mechanism. Environ Prog Sustain Energ 40(6):1–8. https://doi.org/10.1002/ep.13702

Azeez RA, Al-zuhairi FKI (2021) Biosorption of dye by immobilized yeast cells on the surface of magnetic nanoparticles. Alex Eng J 61(7):5213–5222. https://doi.org/10.1016/j.aej.2021.10.044

Bayazit ŞS (2014) Magnetic multi-wall carbon nanotubes for methyl orange removal from aqueous solutions : equilibrium, kinetic and thermodynamic studies. Sep Sci Technol 49(9):1389–1400. https://doi.org/10.1080/01496395.2013.879595

Berni R, Mandlik R, Hausman JF, Guerriero G (2021) Silicon-induced mitigatory effects in salt-stressed hemp leaves. Physiol Plant 171(4):476–482. https://doi.org/10.1111/ppl.13097

Chimeni DY, Hirschberg V, Dubois C, Rodrigue D (2018) Rheological behavior of composites made from linear medium-density polyethylene and hemp fibers treated by surface-initiated catalytic polymerization. Rheol Acta 57(6):445–457. https://doi.org/10.1007/s00397-018-1089-5

Cramer NL (1985) In Proceedings of the 1st international conference on genetic algorithms. L. Erlbaum Associates Inc, USA. https://doi.org/10.5555/645511.657085

Dai D, Fan M (2010) Characteristic and performance of elementary hemp fibre. Mater Sci Appl 01(06):336–342. https://doi.org/10.4236/msa.2010.16049

Darwish AAA, Rashad M, AL-Aoh HA, (2019) Methyl orange adsorption comparison on nanoparticles: Isotherm, kinetics, and thermodynamic studies. Dyes Pigm 160:563–571. https://doi.org/10.1016/j.dyepig.2018.08.045

Dinçel NGK (2022) Determination of oil ratio and fatty acid composition of the seed obtained from the cannabis plant grown in Sivas ecological conditions in the first production year. J Erciyes Agric Anim Sci. https://doi.org/10.55257/ethabd.1081704

Fallahpour A, Olugu EU, Musa SN, Khezrimotlagh D, Wong KY (2016) An integrated model for green supplier selection under fuzzy environment: application of data envelopment analysis and genetic programming approach. Neural Comput Appl 27(3):707–725. https://doi.org/10.1007/s00521-015-1890-3

Feli M, Abdali-Mohammadi F (2019) A novel recursive backtracking genetic programming-based algorithm for 12-lead ECG compression. SIViP 13(5):1029–1036. https://doi.org/10.1007/s11760-019-01441-4

Ferreira, C. Complex Systems **13**, 2 (2001). *arXiv preprint cs/0102027*.

Gan Z, Chow TWS, Chau WN (2009) Clone selection programming and its application to symbolic regression. Expert Syst Appl 36:3996–4005. https://doi.org/10.1016/j.eswa.2008.02.030

Joudi M, Nasserlah H, Mouldar J, Hatimi B, El Mhammedi MA, Bakasse M (2020) Synthesis of an efficient hydroxyapatite – chitosan – montmorillonite thin film for the adsorption of anionic and cationic dyes : adsorption isotherm, kinetic and thermodynamic study. SN Applied Sci 2(6):1–13. https://doi.org/10.1007/s42452-020-2848-3

Karaboğa, D (2017) Yapay Zeka Optimizasyon Algoritmalari. Nobel Akademi Yayıncılık.

Keshavarz A, Mehramiri M (2015) New Gene Expression Programming models for normalized shear modulus and damping ratio of sands. Eng Appl Artif Intell 45:464–472. https://doi.org/10.1016/j.engappai.2015.07.022

Khwannimit D, Maungchang R, Rattanakit P (2020) Green synthesis of silver nanoparticles using *Clitoria ternatea* flower: an efficient catalyst for removal of methyl orange. J Environ Anal Chem. https://doi.org/10.1080/03067319.2020.1793974

Koza JR (1994) Genetic programming as a means for programming computers by natural selection. Stat Comput 4(2):87–112. https://doi.org/10.1007/BF00175355

Lafi R, Abdellaoui L, Montasser I, Hafiane A (2020) Removal of methyl orange from aqueous solution onto modified extracted cellulose from Stipa Tenacissima L. J Environ Anal Chem. https://doi.org/10.1080/03067319.2020.1845663

Li X, Wang G, Li W, Wang P, Su C (2015) Adsorption of acid and basic dyes by sludge-based activated carbon: isotherm and kinetic studies. J Cent South Univ 22:103–113. https://doi.org/10.1007/s11771-015-2500-3

Li H, Wong, ML (2015) Financial fraud detection by using grammar-based multi-objective genetic programming with ensemble learning. In: 2015 IEEE congress on evolutionary computation, CEC 2015-proceedings 1113–1120. https://doi.org/10.1109/CEC.2015.7257014

Liu J, Wang X (2013) Novel silica-based hybrid adsorbents: Lead(II) adsorption isotherms. Sci World J 2013:897159. https://doi.org/10.1155/2013/897159

Liu L, Shao L, Li X, Lu K (2016) Learning spatio-temporal representations for action recognition: a genetic programming approach. IEEE Trans Cybern 46(1):158–170. https://doi.org/10.1109/TCYB.2015.2399172

Madjene F, Chergui A, Trari M (2016) Biosorption of Ni(II) by fig male: optimization and modeling using a full factorial design. Water Environ Res 88(6):540–547. https://doi.org/10.2175/106143016x14504669768859

Magdy YM, Altaher H, ElQada E (2018) Removal of three nitrophenols from aqueous solutions by adsorption onto char ash: equilibrium and kinetic modeling. Appl Water Sci 8(1):1–15. https://doi.org/10.1007/s13201-018-0666-1

Mahmoodi NM, Chamani H, Kariminia HR (2016) Functionalized copper oxide–zinc oxide nanocomposite: synthesis and genetic programming model of dye adsorption. Desalin Water Treat 57(40):18755–18769. https://doi.org/10.1080/19443994.2015.1094677

Moraglio A, Krawiec K, Johnson CG (2012) Geometric semantic genetic programming. Lecture Notes in Computer Science (Including Subseries Lecture Notes in Artificial Intelligence and Lecture Notes in Bioinformatics) 7491 LNCS (PART 1):21–31. https://doi.org/10.1007/978-3-642-32937-1_3

Muduli PK, Das SK (2014) CPT-based seismic liquefaction potential evaluation using multi-gene genetic programming approach. Indian Geotech J 44(1):86–93. https://doi.org/10.1007/s40098-013-0048-4

Muduli PK, Das MR, Das SK, Senapati S (2015) Lateral load capacity of piles in clay using genetic programming and multivariate adaptive regression spline. Indian Geotech J 45(3):349–359. https://doi.org/10.1007/s40098-014-0142-2

Nguyen DTC, Van TT (2022) A chemometric approach based on Box-Behnken and response surface methodology for design and optimization of ciprofloxacin adsorption from water. Chem Pap 76(8):4873–4883. https://doi.org/10.1007/s11696-022-02207-y

Nguyen S, Mei Y, Zhang M (2017) Genetic programming for production scheduling: a survey with a unified framework. Complex Intell Syst 3(1):41–66. https://doi.org/10.1007/s40747-017-0036-x

Okpara OG, Ogbeide OM, Ike OC, Menechukwu KC, Ejike EC (2021) Optimum isotherm by linear and nonlinear regression methods for lead (II) ions adsorption from aqueous solutions using synthesized coconut shell–activated carbon (SCSAC). Toxin Rev 40(4):901–914. https://doi.org/10.1080/15569543.2020.1802596

Pan I, Pandey DS, Das S (2013) Global solar irradiation prediction using a multi-gene genetic programming approach. J Renew Sust Energ Rev. DOI 10(1063/1):4850495

Poli R, Langdon WB, McPhee NF (2008) A Field Guide to Genetic Programing. In Wyvern (Issue March). http://www.essex.ac.uk/wyvern/2008-04/Wyvern April 08 7126.pdf

Riaz Q, Ahmed M, Zafar MN, Zubair M, Nazar MF, Sumrra SH, Ahmad I, Hosseini-Bandegharaeic A (2022) NiO nanoparticles for enhanced removal of methyl orange: equilibrium, kinetics, thermodynamic and desorption studies. J Environ Anal Chem 102:1–20. https://doi.org/10.1080/03067319.2020.1715383

Runjavec ŠM, Domanovac MV, Meštrović E (2022) Removal of organic pollutants from real pharmaceutical industrial wastewater with environmentally friendly processes. Chem Pap 76(3):1423–1431. https://doi.org/10.1007/s11696-021-01919-x

Searson DP, Leahy DE, Willis MJ (2010) GPTIPS:An open source genetic programming toolbox for multigene symbolic regression. In: Proceedings of the international multiconference of engineers and computer scientists IMECS, December, pp 77–80.

Sriram G, Bendre A, Altalhi T, Jung H, Hegde G (2022) Surface engineering of silica based materials with Ni–Fe layered double hydroxide for the efficient removal of methyl orange : Isotherms, kinetics, mechanism and high selectivity studies. Chemosphere 287:131976. https://doi.org/10.1016/j.chemosphere.2021.131976

Su Y, Jiao Y, Dou C, Han R (2014) Biosorption of methyl orange from aqueous solutions using cationic surfactant-modified wheat straw in batch mode. Desalin Water Treat 52(31–33):6145–6155. https://doi.org/10.1080/19443994.2013.811121

Subbaiah MV, Kim DS (2016) Adsorption of methyl orange from aqueous solution by aminated pumpkin seed powder: Kinetics, isotherms, and thermodynamic studies. Ecotoxicol Environ Saf 128:109–117. https://doi.org/10.1016/j.ecoenv.2016.02.016

Suganuma M, Shirakawa S, Nagao T (2018) A genetic programming approach to designing convolutional neural network architectures. IJCAI International Joint Conference on Artificial Intelligence. https://doi.org/10.24963/ijcai.2018/755

Tofan L, Paduraru C, Toma O (2016) Zinc remediation of aqueous solutions by natural hemp fibers: Batch desorption/regeneration study. Desalin Water Treat 57(27):12644–12652. https://doi.org/10.1080/19443994.2015.1052566

Viscusi G, Barra G, Verdolotti L, Galzerano B, Viscardi M, Gorrasi G (2019) Natural fiber reinforced inorganic foam composites from short hemp bast fibers obtained by mechanical decortation of unretted stems from the wastes of hemp cultivations. Mater Today Proc 34:176–179. https://doi.org/10.1016/j.matpr.2020.02.672

Wu L, Liu X, Lv G, Zhu R, Tian L, Liu M, Li Y, Rao W, Liu T, Liao L (2021) Study on the adsorption properties of methyl orange by natural one-dimensional nano-mineral materials with different structures. Sci Rep 11(1):1–11. https://doi.org/10.1038/s41598-021-90235-1

Zhu J, Yi J, Kang Q, Huang J, Cui Y, Zhang G, Wang Z, Zhang L, Zheng Z, Lu J, Hao L (2021) Anti-fatigue activity of hemp leaves water extract and the related biochemical changes in mice. Food Chem Toxicol 150:112054. https://doi.org/10.1016/j.fct.2021.112054